Molecular Crystals and Liquid Crystals Science and Technology. Section A. Molecular Crystals and Liquid Crystals
Publication details, including instructions for authors and subscription information:
http://www.tandfonline.com/loi/gmcl19

Structure and Defects in Liquid Crystals from Electron Diffraction and High Resolution Imaging

I. G. Voigt-martin [a], M. Schumacher [a], M. Honig [a], P. Simon [a] & R. W. Garbella [a]
[a] Inst. of. Physical Chemistry, University of Mainz, FRG

Version of record first published: 24 Sep 2006.

To cite this article: I. G. Voigt-martin , M. Schumacher , M. Honig , P. Simon & R. W. Garbella (1994): Structure and Defects in Liquid Crystals from Electron Diffraction and High Resolution Imaging, Molecular Crystals and Liquid Crystals Science and Technology. Section A. Molecular Crystals and Liquid Crystals, 254:1, 299-320

To link to this article: http://dx.doi.org/10.1080/10587259408036083

Mol. Cryst. Liq. Cryst. 1994, Vol. 254, pp. 299–320
Reprints available directly from the publisher
Photocopying permitted by license only

Printed in the United States of America

STRUCTURE AND DEFECTS IN LIQUID CRYSTALS FROM ELECTRON DIFFRACTION AND HIGH RESOLUTION IMAGING

I.G. VOIGT-MARTIN, M. SCHUMACHER, M. HONIG, P. SIMON, R. W. GARBELLA
Inst. of. Physical Chemistry, University of Mainz, FRG

(Received: February 7, 1994)

INTRODUCTION

The mesophases formed by liquid crystals can be divided into four main groups: (a) Nematic, (b) Discotic, (c) Smectic, (d) Sanidic. Because there is very little structural information in the nematic phase (a), we describe here our work on the other three mesophases. While the monomers generally crystallize when quenched into the solid state, the polymers can be made to retain their mesophase structure by forming a glass. Therefore this phase becomes amenable to high resolution imaging.

Since the desired physical properties of any material depend on the structural details at a molecular level, it is essential to understand the relationship between them in order to synthesize the most suitable molecules. The purpose of this paper is to demonstrate that the tremendous advances in computer technology which have been made recently can be used to great advantage in modern electron microscopy and diffraction on condition that certain theoretical facts are fully understood and the line of approach is adapted to the specific problem. The purpose of this paper is to give other investigators insight into our approach based electron-microscopical methods and hopefully to trigger new impulses.

Because both short range and long range orientational and translational correlations are lower in the mesophase, the number of reflections is severely reduced and structural analysis along traditional lines becomes impossible.

EXPERIMENTAL PROCEDURE

The approach adopted in this work is described in the following:

I. Choice of suitable samples.

Three typical representatives from the major mesophases were chosen:

(A) Triphenylene derivatives with ether and ester linkages to the aliphatic chains

(B) Smectic C chiral biphenyl nitrohydroxy benzoic acid

(C) Sanidic polyamide

II. Electron Diffraction

Typical electron and X-ray diffraction patterns associated with these samples are shown in the schematic diagram Fig. 1.

Although the number of reflections is minimal, even such a limited diffraction pattern gives more information than the long spacing, provided that the implications of scattering theory are understood.

In order to study the structure of liquid crystals it is necessary to consider the statistical distribution of molecular positions described by the correlation function in real space $g_2(r)$. This can be obtained from its Fourier Transform, the measured scattering function S(q), both in radial q_r and tangential q_t direction. S(q) is also referred to as the shape factor. The particular characteristics of this function have been calculated and measured for monomeric smectics[1] and discotics[2] and are known to produce very sharp peaks (δ functions) with an algebraic decay only in the wings of the intensity maximum, which is related to the elastic properties of the material.

The line shape and contour plot of the observed small angle maxima of the investigated polymeric liquid crystals are shown in Fig. 2.

These results show the following important structural features:

(A) Discotic polymer.

Six hexagonally arranged and usually sharp reflections compared with normal polymers. Nevertheless, there is some slight broadening giving a Gaussian distribution. The contour plots are circular, indicating that the defects are isotropically arranged.

(B) Smectic polymer.

The small angle maxima are very sharp in the radial direction but frequently have streaks in a tangential direction indicating disturbances

in the translational correlations arising from planes perpendicular to this direction. The defects are therefore not isotropically distributed.

(C) Sanidic polymer.

The diffraction pattern is biaxial. The small angle maximum is generally not as sharp and can be represented by a Lorentz distribution in the radial direction. There is also broadening tangentially, which can sometimes be resolved sufficiently well to reveal two satellites. The loss of translation correlations therefore extends in at least 2 directions.

This information from the small angle maxima is therefore very informative but for a deeper understanding of the relationship between physical properties and molecular architecture, more detailed structural information is required. In particular, it is important to understand how the mesogenic units pack without the disturbing influence of the polymer chain.

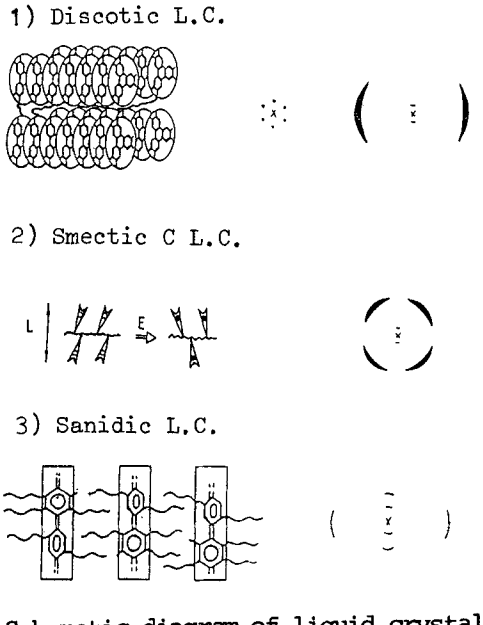

Schematic diagram of liquid crystals with associated diffraction pattern

Fig.1

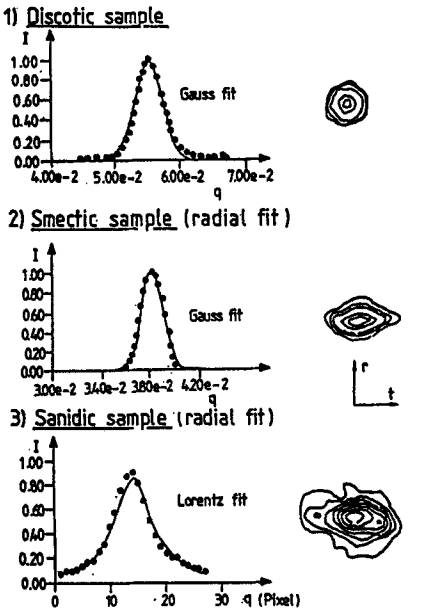

Line profile analysis and contour plots of liquid crystalline polymers.

Fig.2

The procedure adopted was as follows:

I Electron Diffraction

(1) Analysis of electron diffraction pattern obtained from crystalline monomers

Structural analysis based on direct phase methods[4] and on maximum entropy and log likelihood statistics[5] have been applied very successfully to electron crystallography in recent years[6-8] and these are undoubtedly the best methods when they can be applied. However, a large number of accurate intensities is required. These are never available in liquid crystals. Over and above this, crystallography methods apply to the perfect crystal, whereas the defects are of interest in liquid crystals.

(2) Observation of the transition from crystal to liquid crystalline mesophase

(3) Comparison of diffraction pattern from monomeric and polymeric mesophases.

II. Analysis of high resolution images.

Crystallography provides information at an atomic level about perfect crystals. However, the properties of liquid crystals depend on their defects and these can be revealed at a molecular level by electron microscopy.

We have described in previous papers the difficulties associated with obtaining high resolution images from beam sensitive samples[9, 10]. In addition to these experimental difficulties, phase contrast imaging involves the choice of a suitable contrast transfer function for the specific smectic, discotic or sanidic sample investigated, whose only structural features are in the small angle range. We have shown some years ago that a highly unusual phase transfer function $\chi(q)$ must be chosen to image these features[11, 12] and have proved theoretically that for these samples under the chosen transfer conditions the image intensity distribution I(R) is given by:

$$I(R) = 1 - 2\sigma < V_p(R) >$$

where σ is $\pi/\lambda E$, λ is the electron wave length, E is the accelerating voltage, $V_p(R)$ is the projected potential of the object

Therefore, by using the technique of phase contrast imaging at unusually large defocus values which we suggested some years ago[10, 12] an image of the projected potential in the sample is obtained. The transfer function can be correctly estimated by calculating the Fourier Transform of the image on-line. However, both diffraction pattern and images must be simulated in order to ensure correct interpretation.

III. Conformation of molecule and simulation of diffraction pattern.
The procedure adopted in our work is as follows:
(1) The molecular conformation is calculated using semi-empirical quantum mechanical methods. Normally parts of the mesogenic group whose conformation is known from the literature are used as starting conformation, gradually further molecules are added and the energy minimized using MM2 force field calculations. This whole molecule is then used as a starting conformation for MOPAC 6.0 calculations on an IBM RISC RS6000. Generally several energy minima are found. All of them must be subjected to the procedures described in the following.
(2) The molecule is placed in the unit cell using CERIUS 3.2. The space group for simulation is chosen on the basis of the experimentally observed crystal dimensions, symmetry relations and systematic absences. Care is taken in the experiments to avoid dynamical scattering.
(3) The calculated diffraction pattern is compared with the experimental one. If agreement is poor, it may be necessary to try an alternative molecular conformation.
(4) The model structure from the crystal now gives detailed information about the scattering from individual parts of the molecule. On approaching the l.c. phase, disorder first arises in the alkane chains and can be simulated in the programs.
(5) Finally the effect of dynamical scattering on the intensities is included in the calculation.

IV. Simulation of high resolution image
Using the coordinates of all the atoms calculated in the previous step the electron wave function after interaction with all the atoms in the sample is calculated in subsequent thin slices until the wave function emerging at the exit plane is obtained. Clearly this involves an enormous mathematical effort, for which several procedures are now available[14,15]. In the MULTISLICE procedure the iteration is performed in reciprocal space because the wave function exists only at discrete points thus requiring less computer time. In a subsequent-step the experimentally used microscope transfer function is accounted for and the intensity distribution in real space calculated by a second Fourier Transformation. However, it is also possible and in some cases, advantageous to calculate the entire phase grating transmission function in real space, as is done in the VAN DYCK procedure adopted here.

Thus the entire procedure of analysis is performed by a series of interlinked computers as shown in Fig. 3.

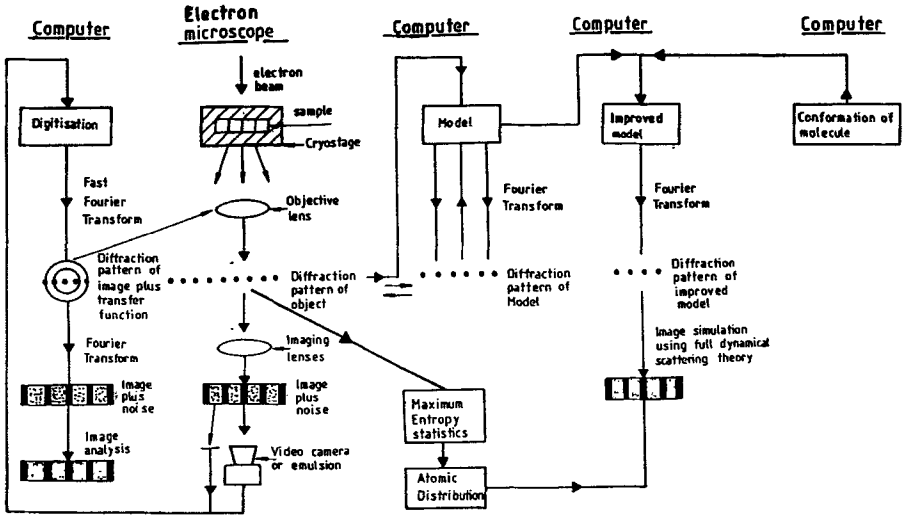

Fig. 3 Procedure used for high resolution electron microscopy, crystallographic determination and image simulation.

In the following, the analysis of our results for discotic, smectic c and sanidic polymers will be described. The procedure for discotics are described in more detail because the other materials were then investigated in the same manner.

Results

A) DISCOTIC LIQUID CRYSTALS

It is well established that many compounds composed of disc-like molecules have stable thermotropic l.c. phases[17-25].

Recently there has been a revival of interest in thin films of disc shaped molecules because they have been shown to have photoconducting properties in the mesophase but not in the crystalline phase[16]. X-ray analysis of crystalline strands revealed different crystallographic space groups, depending on the details of molecular architecture[20, 23]. In this work an attempt is made to understand the relationship between molecular orientation and film plane in the non-conducting crystalline phase as well as in the l.c. phase and furthermore, to understand the nature of the defects which affect this physical property.

For this purpose, two closely related triphenylene samples were analyzed, namely a triphenylene ether (a) a triphenylene ester (b) and their polymeric analogs (c) (Fig. 4)

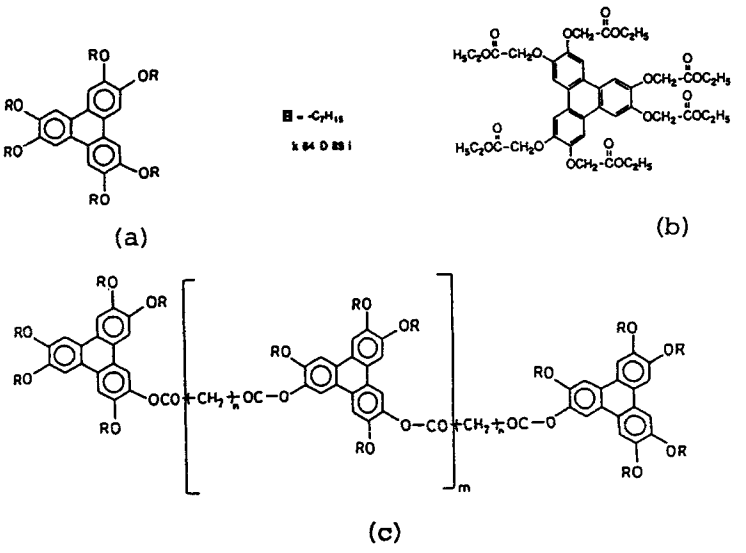

Fig 4 Moleculare architecture of discotic molecules.

The main distinguishing feature between the two molecules is the doubly bounded oxygen atom in the ester.

Electron diffraction from l.c. phase

The character of the diffraction patterns from both monomers and polymers in the l.c. phase are shown in Fig. 5.

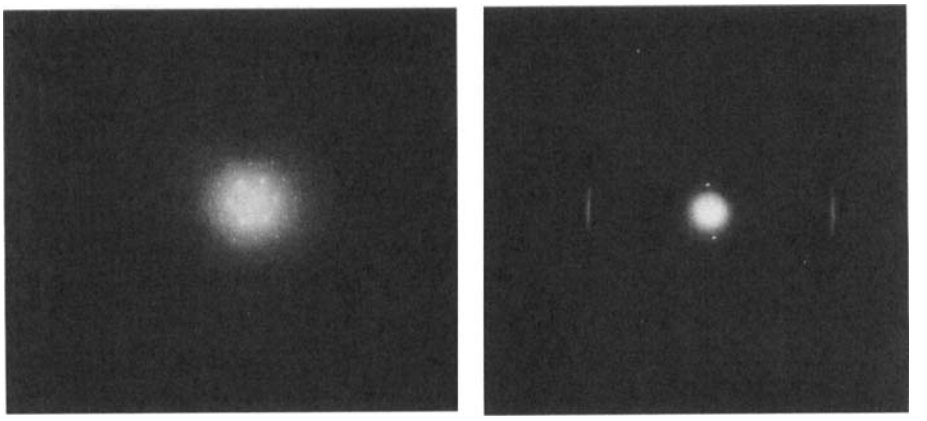

(001) zone (100) zone

Fig 5 Electron diffraction patterns from discotic triphenylenes

In the [001] zone a hexagonal arrangement of very sharp reflections with only one higher order is observed, whereas in the [100] zone there are 2 sharp small angle maxima and an oriented halo in the wide angle region. In a general way it is possible to postulate that the [001] zone reveals hexagonally arranged columns viewed from above with lattice constants of about 22Å and the [100] zone reveals columns composed of individual discs at a spacing of 3.5Å viewed from the side. The cell constants for the monomer in the l.c. phase are:

Triphenylene hexaether	monomer: a=b=22.6Å,	α=β=90°,	γ=120°
	polymer: a=b=23Å,	α=β=90°,	γ=120°
Triphenylene ester	monomer: a=b=19.05Å,	α=β=90°,	γ=120°

Electron diffraction from the crystalline phase

The electron diffraction patterns from the same zones in the crystalline phases of the triphenylene ether (Fig. 6) and the triphenylene ester (Fig. 7) are much more revealing.

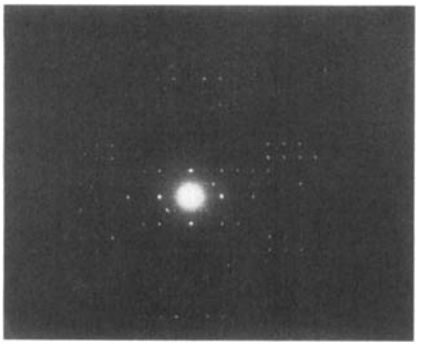

Electron diffraction pattern of crystalline hexaheptyloxy-triphenylene in (001) zone.

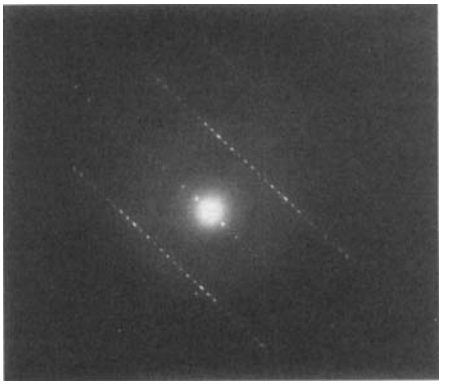

Electron diffraction pattern of crystalline hexaheptyoxy-triphenylene in (100) zone.

Fig.6

In the [001] zone the triphenylene ether is orthogonal, while the ester has hexagonal symmetry. The cell constants of the crystalline ether are a=32.6Å, b=38.3Å, c=5Å, α=β=γ=90° that of the crystalline ester are a=b=18.8Å, c=14.2, α=β=90°, γ=120°. Therefore, there is a superstructure in the ab plane of the ether and in bc plane of the ester. In the [100] zone the first layer line of the ether is at a distance of 5.2Å from the equator and the (015) are the strongest reflections on the first layer line. In contrast to this, the strongest reflection of the ester is the (004) reflection at 3.5Å, indicating a superstructure of 14Å in the bc projection.

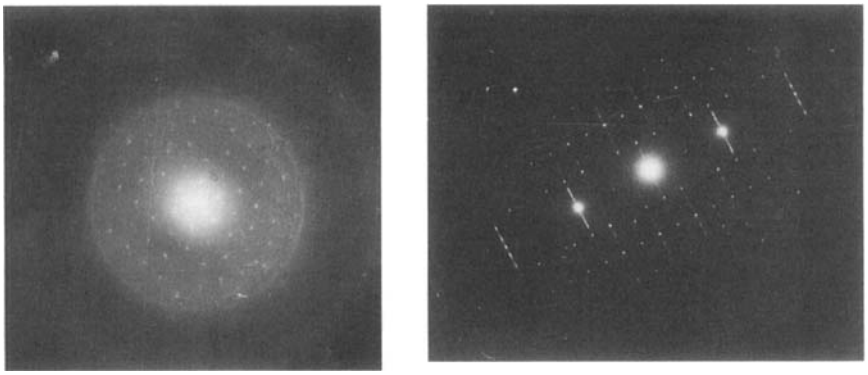

Electron diffraction pattern of crystalline triphenylene ester in [001] zone

Electron diffraction pattern of crystalline triphenylene ester in (100) zone

Fig.7

Conformation of molecule and simulation of electron diffraction patterns

The model structures found by choosing the most suitable low energy conformations[26] and the space groups based on experimental cell dimensions and systematic absences are shown in the top left hand corner of Fig. 8 and 9. The calculated diffraction patterns are shown from three different zones.

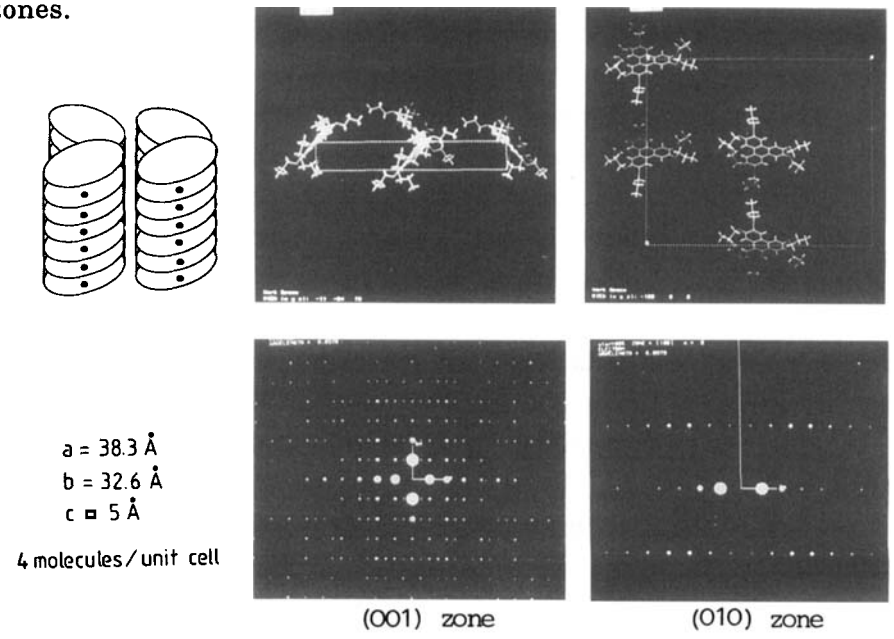

Fig 8

Structural model of triphenylene ether with diffraction patterns from different zones.

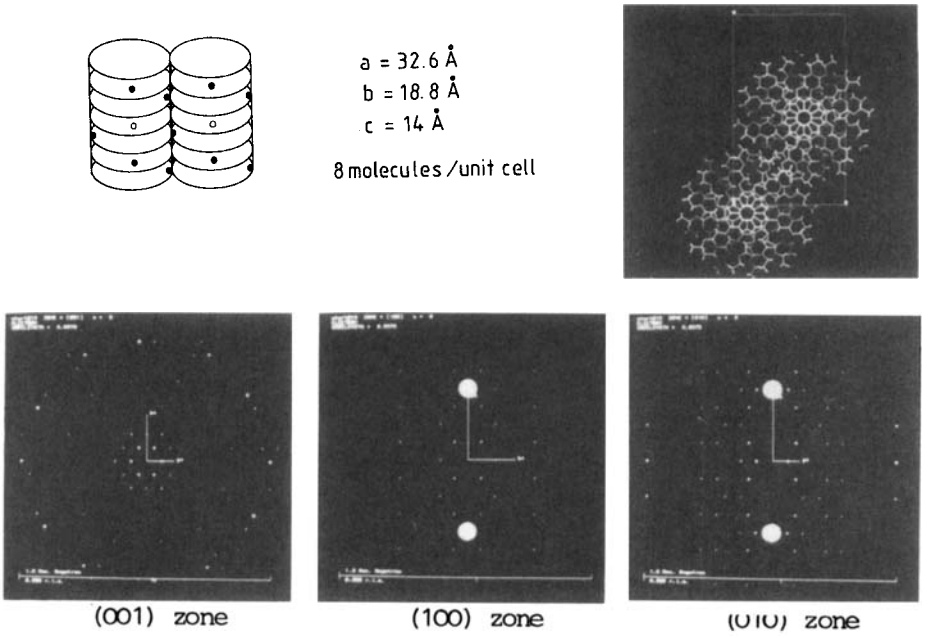

Structural model of triphenylene ester with diffraction patterns from different zones.

Fig. 9

The agreement between experiment and calculation is good and shows the major important features; namely that the triphenylene ethers are tilted, thereby losing their hexagonal symmetry in the ab projection, giving rise to a unit cell with C2 symmetry. In the triphenylene ester, the conformational analysis showed that the doubly bonded oxygen projects out of the molecular plane such that the discs cannot stack directly above one another and a helical superstructure is formed.

The analysis of electron diffraction patterns therefore show that in discotic molecules different superstructures arise both in ab and bc projections, depending on details of molecular architecture (Fig. 10).

When the samples are heated into the mesophases, the aliphatic chains are subjected to conformational changes and the discs begin to rotate so that, in both projections, all superstructural details are lost and only the average projected positions of molecular columns are relevant in scattering.

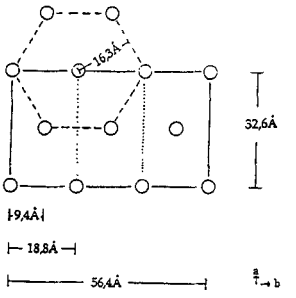

Superstructure Triphenylene ether.

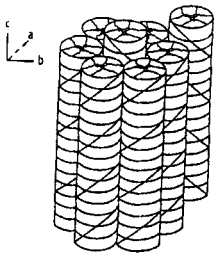

Superstructure Triphenylene ester.

Fig 10

High resolution images

Typical high resolution images of triphenylene ethers and esters are shown in Figs. 11, 12 and described in detail elsewhere[3, 27]

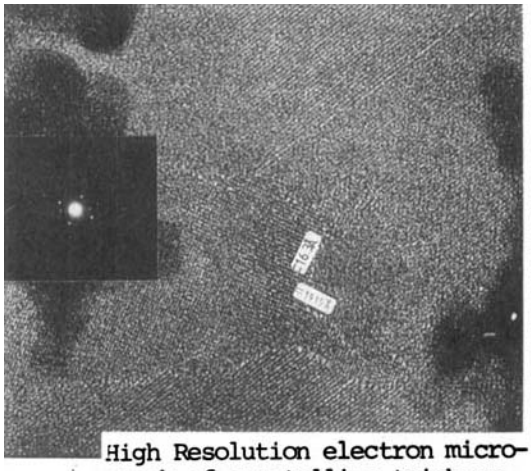

High Resolution electron micrograph of crystalline triphenylene monomer with microdiffraction .

Fig 11

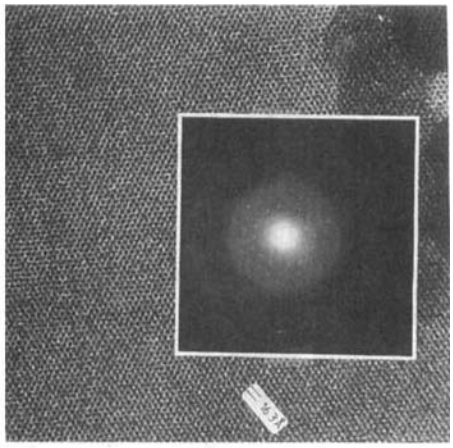

High resolution electron micrograph of triphenylene hexaester showing the c-zone axes.

Fig. 12

The images show the molecules in the a,b projection with orthorhombic and hexagonal symmetry, as expected from the diffraction patterns. In addition, the images indicate typical defects, namely dislocations and grain boundaries. In contrast to this, in the quenched liquid crystalline polymer, the molecular columns always lie with their cylinder axis perpendicular to the film plane and grain boundaries are never observed.

However, while quasi long range order is preserved, there are disturbances in short range order (Fig. 13).

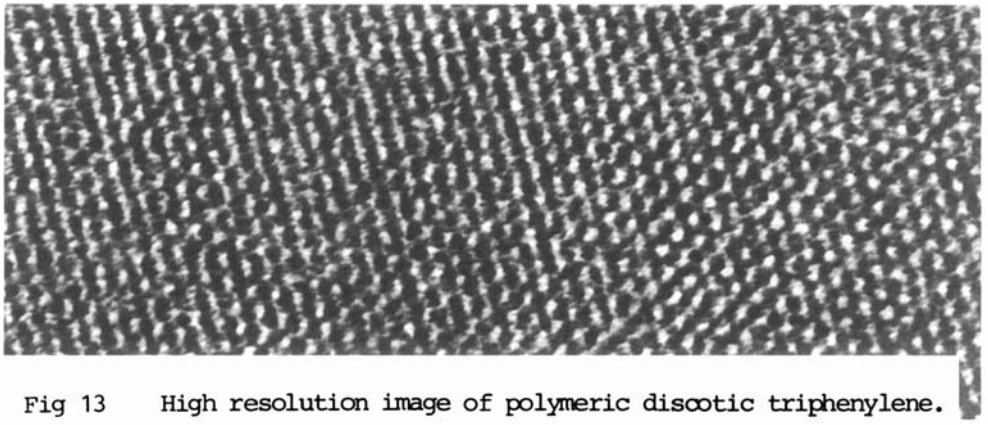

Fig 13 High resolution image of polymeric discotic triphenylene.

Quantitative characterisation of molecular deviations in liquid crystals

The most effective way of quantitatively characterising the deviations of the molecular positions from perfect lattice positions is by calculating the cross-correlation functions. We have described the mathematical procedure elsewhere[11]. The result is shown in Fig. 14. The cross-correlation map shows the deviations of the molecules in the l.c. phase from perfect lattice positions. The deviation vectors clearly show that deciations only fractions of a lattice constant in translation and rotation arise. These disturbances in short range correlations lead to the loss of higher order maxima in the diffraction patterns. In this way, lattice strains are not built up so that there are no grain boundaries. Quasi long range order is retained, therefore the small angle reflections are sharp.

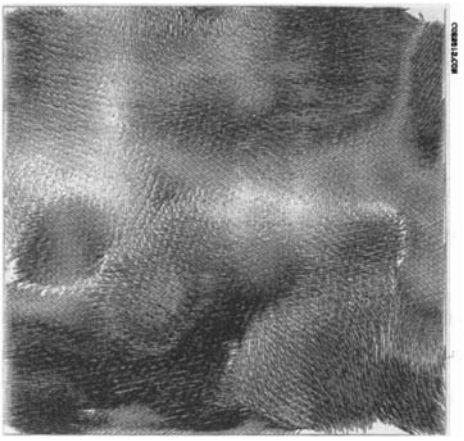

Fig 14 Deviation vectors obtained by cross-correlation of discotic "lattice" with perfect crystal.

Simulation of images

The relationship between the object and the observed image was established by simulation procedures which we have described elsewhere[3], as shown in Fig. 15.

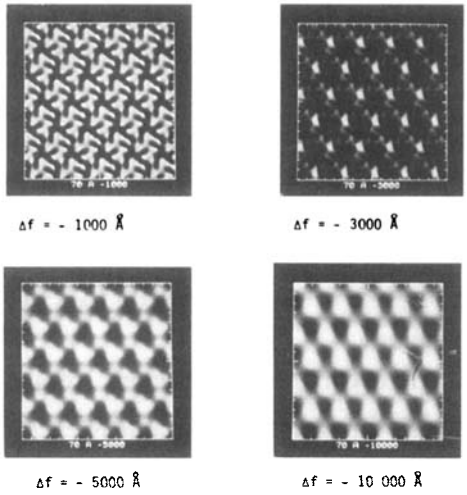

Fig. 15 Simulated images of triphenylene crystals sa a function of defocus value Δf.

The series shows that the image is NOT a direct picture of the object but the result of interference between electron beams, as well as many scattering processes in the sample and the effects of the electron microscope lenses[28]. The calculated image using the experimental microscope functions and sample thickness corresponds to the picture in the bottom right hand corner.

B) SMECTIC C* LIQUID CRYSTALS

Ferroelectric liquid crystals owe their important switching characteristics to the fact that the individual molecules with a dipole moment μ are non centro-symmetric and that their mutual orientation in the smectic c* phase in which the molecular director n has a tilt angle θ with respect to the layer normal s does not give rise to a centro symmetric super-structure. This breaking of symmetry[29] is essential and can be achieved by introducing a chiral molecule into a surface stabilized cell with a gap width of 2μm-10μm, and suppressing the conical degeneracy of the molecules such that the resultant polarisation P does not have any component along n.

When the sample is subjected to an alternating field, the molecules are forced to move on a cone so that the dipole can change direction[30].

From this short summary it is clear that massive collective motion is required during switching, and that this is very difficult to visualize in polymers, whose molecules tend to adopt a random conformation. However, in recent years, polymers have been synthesized which demonstrate a Goldstone mode in dielectric experiments and which have a high spontaneous polarization of over 100 nC/cm^2 [31-34].

In order to gain insight into this phenomenon at a molecular level, it is necessary to relate n, s, μ and P. The value of μ can be obtained by conformational calculation using semiempirical quantum mechnical methods as described in the introduction. Both n and s can be obtained from structure analysis using the crystal structure as a guide to a better understanding of the liquid crystal reflections.

The chemical structure of the monomeric molecules and their polymeric analogs chosen for this investigation is shown in Fig. 16:

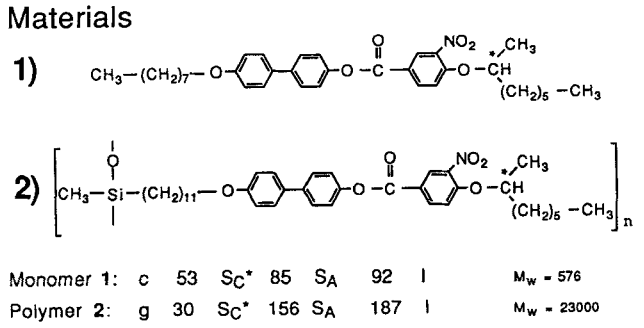

Fig 16

The samples were heated into the smectic c* phase in an a.c. field (5-60Hz, monomer 2000 Vcm^{-1}; polymer 10 000 Vcm^{-1}) producing a spontaneous polarisation P of 150 nC/cm^2 in both monomer and polymer.

Light and electron microscopy

For an initial characterisation light micrographs were obtained of both monomer and polymer in the ITO cells with the electric field switched on (Fig. 17a,b). In both cases stripes are observed in the highly oriented switching material with a spacing of 20 μm in the monomer and 2 μm in the polymer. In the monomer a further zig-zag modulation within the stripes with a modulation of 0.1 μm is present. Electron micrographs revealed that these zig-zag stripes with an included angle of 130° were again subdivided into stripes (Fig. 18).

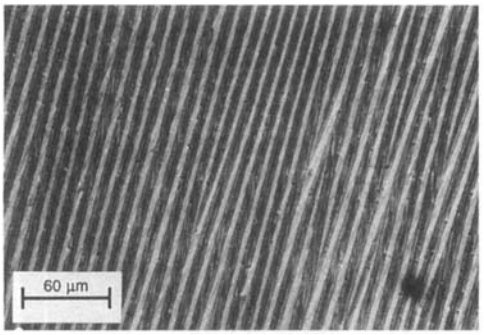

Monomer in dc field (S_C^* -phase, 8V), crossed polarizers.

Fig 17(a)

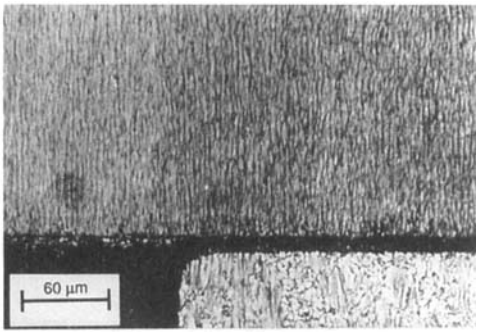

Polymer (2) in dc field (S_C^* - phase, 80V), crossed polarizers.

Fig 17(b)

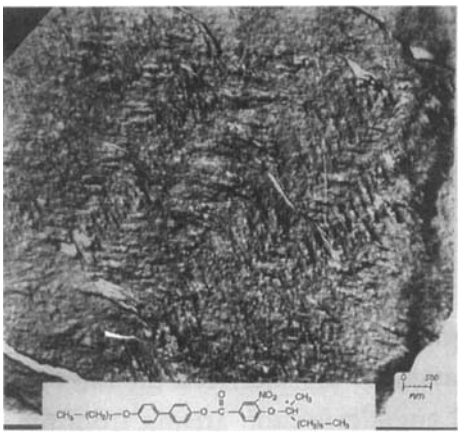

Fig 18. Electron micrograph of replica from monomer (2) showing zig-zag defects.

Electron diffraction

The relationship between the molecular direction n and the layer normal s can be derived from electron diffraction by extracting thin slivers of sample from the quenched cells. (Fig. 19 b,c) and comparing these diffraction patterns with those obtained from a specially oriented crystal (Fig. 19a). The similarities and differences are very obvious and have been highlighted in the schematic drawings above the diffraction pattern.

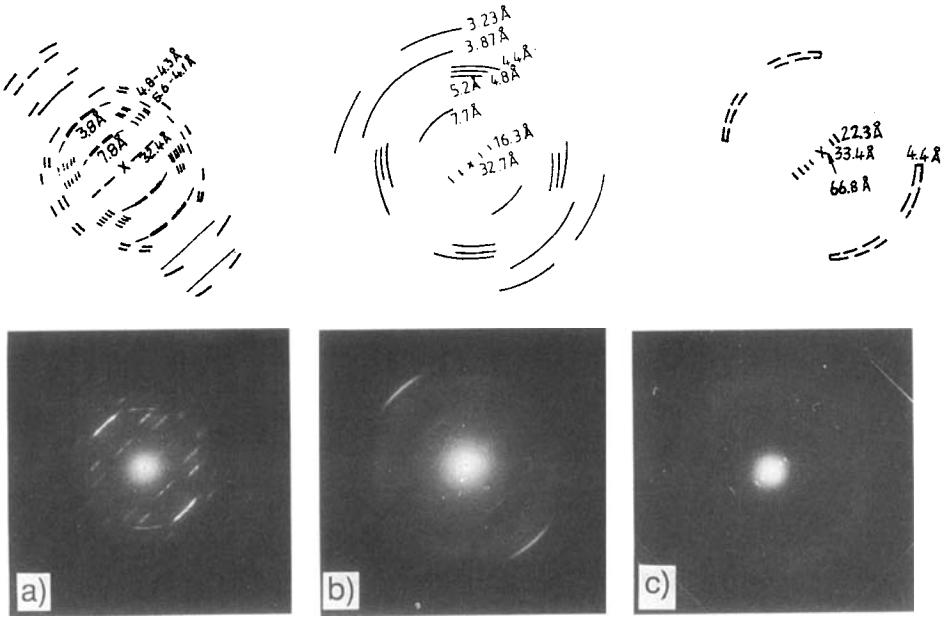

Electron diffraction patterns of monomer (fibre pattern)(a) and thin films of monomer(b) and polymer(2)(c) extracted from ITO-cells.

Fig 19

The split wide angle halo which is observed in the polymer sample can be related to the series of reflections between 4.4-5.2Å in the crystal, arising from the distance between aliphatic chains. The included angle is 50±10°, corresponding to an angle of 130° between the relevant reflecting planes in real space. The small angle reflection arising from the smectic planes and indicating the direction of s have a periodicity of 32.7Å in the monomer and about double this periodicity in the polymer (66.5Å). Using the crystal diffraction patterns, crystal structure simulations were performed as before with CERIUS, using the molecular conformation calculated by MOPAC shown in Fig. 20 and giving a molecular length of 32Å.

These projections are especially included because they clearly show the direction of the dipole with respect to the molecule. Placing this molecule in the cell calculated from the diffraction pattern in the head to head arrangement expected for the polymer (Fig. 21) it can be seen how the dipoles pointing out of the z,y plane must rotate on reversing the field in order to point into the z,y plane, and that this motion requires collective motion of the whole layer due to the bent conformation of the molecule.

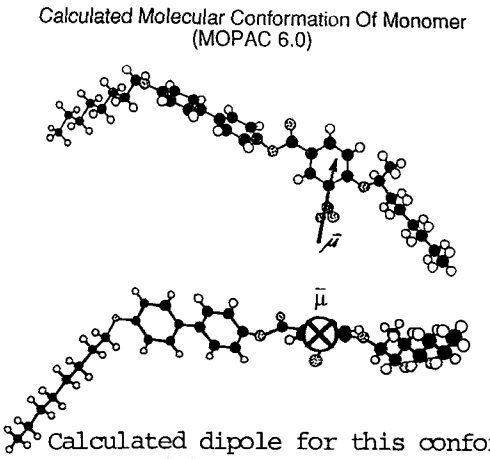

Calculated dipole for this conformation :4.9 Debye.

Fig 20

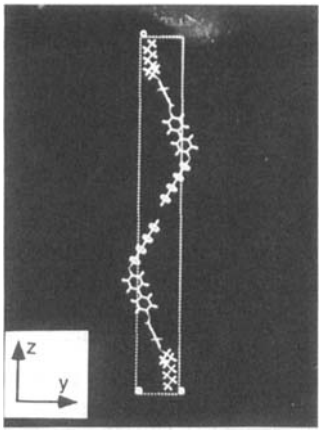

Fig 21

Fig. 22 shows that the main features of the experimental diffraction pattern are well represented by the calculated diffraction pattern.

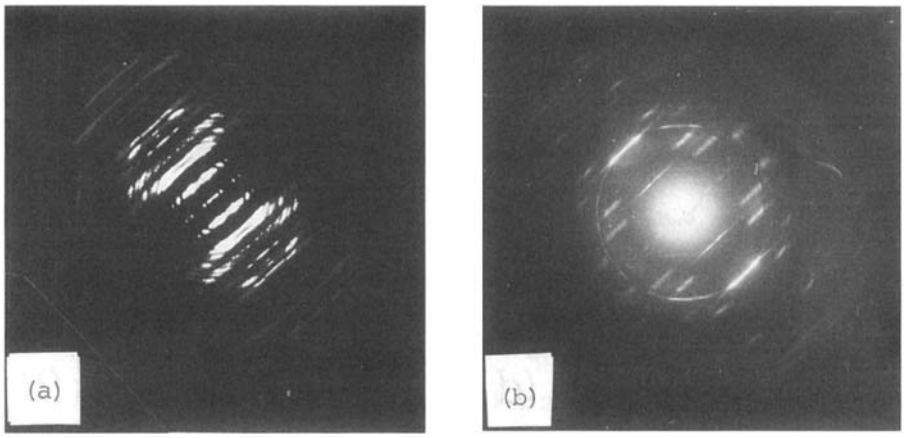

Calculated (a) and experimental (b) electron diffraction patterns (CERIUS™ 3.1)

Fig 22

Sanidic liquid crystals

The interest in this class of materials stems from the attempt to obtain high tensile strength materials by employing highly oriented, stiff macromolecules. The first materials which were synthesised had the undesirable property of having extremely high melting temperatures and very

poor solubilities. In order to rectify this, aliphatic chains were attached to the stiff mesogenic groups and an improvement in these properties achieved[36]. However, the price which had to be paid for these advantages was a reduction in mechanical strength. The reasons for this are to be sought at a molecular level, using structural methods.

As in the previous case, the structural information which can be gleaned from X-ray and electron diffraction is very sparse[37-39]. Generally a biaxial diffraction pattern consisting of only six arced intensity maxima is obtained.

On the basis of such meager experimental evidence, many different model structures can be proposed.

In order to obtain a better understanding of the packing principles involved, monomeric analogs were synthesized[37] and crystallized, so that their diffraction patterns could be compared with that of the polymer. One typical example of this class of materials with structural formula shown below will be described in the following (Fig. 23).

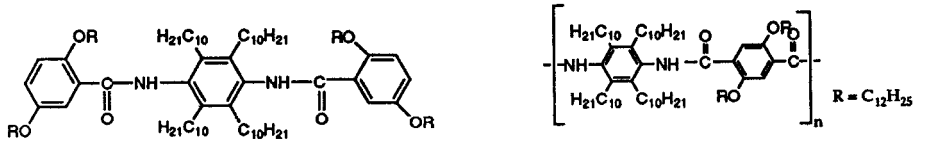

Fig 23

The "monomer" in fact consists of 1,5 structural units.

Electron diffraction from polymeric l.c. phase.

The electron diffraction pattern from the polymeric analog shows the biaxial diffraction pattern familiar for this class of materials (Fig. 24).

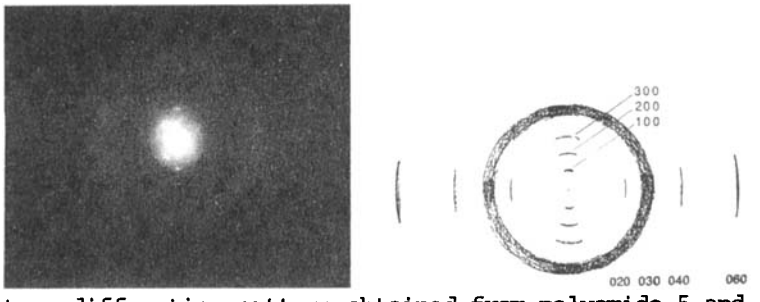

Fig. 24 Electron diffraction pattern obtained from polyamide 5 and its schematic drawing showing indexed diffraction axes.

The small angle maxima whose intensity profile and contour plots were described in the introduction, corresponds to 1/27Å^{-1} and the wide angle spacings to 1/12Å^{-1}.

Electron diffraction from monomer crystals

The samples were oriented by epitaxy and by solution growth so that two perpendicular crystallographic zones could be obtained (Fig. 25).

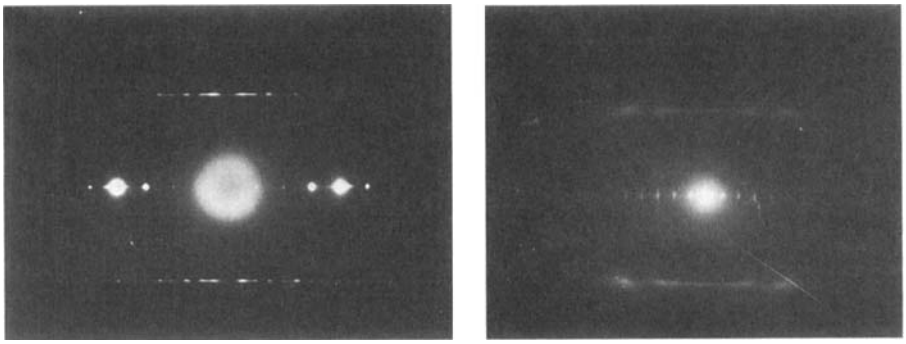

(001) zone (100) zone

Fig 25 Experimental diffraction patters of sanidic samples.

The relevant maxima in the [010] zone are 1/27Å^{-1} and its higher orders. In the [001] zone, the small angle maxima are found at 1/18Å^{-1} and its higher orders. In both cases, the wide angle layer lines are situated at 1/5.36Å^{-1}.

Simulation of electron diffraction patterns

Semi-empirical quantum mechanical calculations of the mesogenic core reveal several energy minima, defining the planes of aromatic rings (Fig. 26).

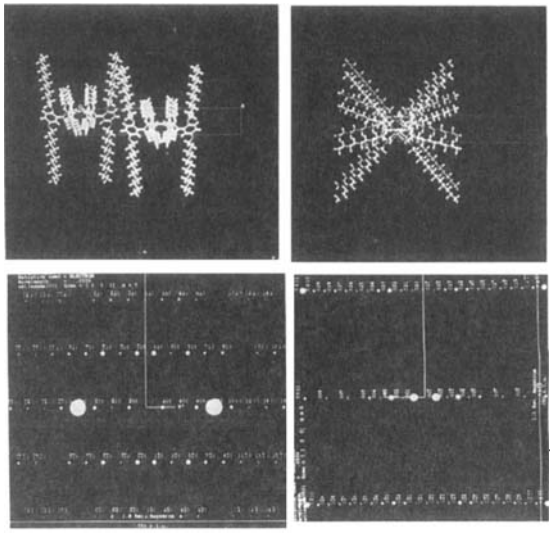

Structural model with calculated diffraction patterns.

Fig 26

This conformation will have a dramatic influence on the angle at which the aliphatic chains project from the core. All these conformations were tested until the correct crystal structure was obtained .

High resolution images

We have shown previously how high resolution images were obtained from a similar material[37]. By choosing the transfer function appropriate for the 18Å and the 28Å spacings determined from the diffraction patterns it was possible to obtain high resolution images from both monomer and its polymeric analog (Fig. 27 and 28).

The images indicate the reason for nature of the diffraction pattern. While the crystalline molecular planes are perfectly oriented, the l.c. phase has developed only small quadratic blocks of poorly oriented material surrounded by non-oriented regions.

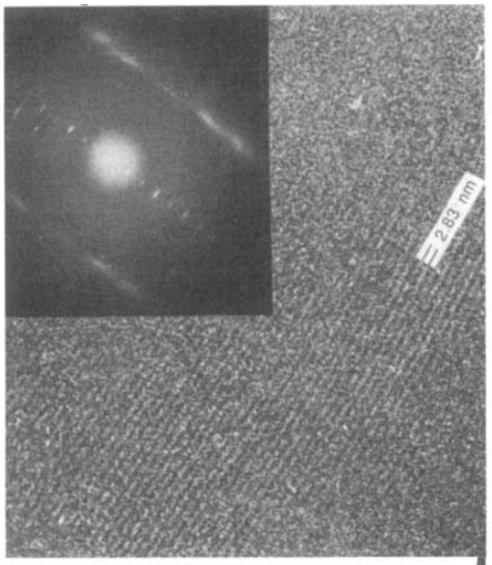

Fig. 27 High resolution image of crystal.

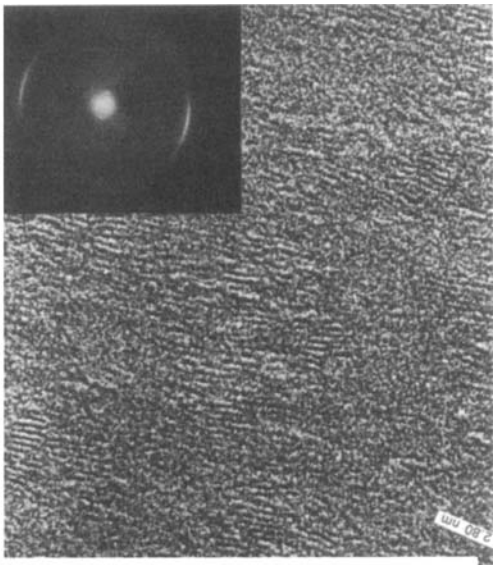

Fig. 28 High resolution image of corresponding sanidic sample.

Conclusions

The crystalline diffraction patterns have given clear information about the molecular conformation and packing. From the molecular and unit cell dimensions, it is clear that 3 projections have been studied, as indicated below (Fig. 29).

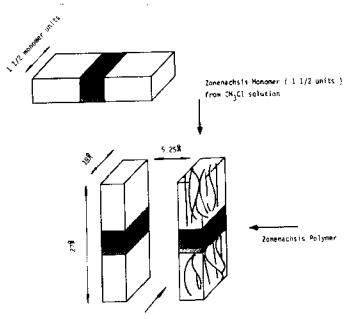

Fig 29 Model structures of sanidic samples showing relevant projections.

The high resolution images from this sanidic material and others similar to it show that it is difficult to achieve good orientation thoughout the whole sample, so that mechanical stress is not transferred only to the polymer backbone. We have shown elsewhere that it is possible to achieve better orientation with other molecules, but the main features are generally of this nature and responsible for the disappointing mechanical strength.

Literature

[1] J. Als-Nielsen, J. D. Litser, R. J. Birgeneau, M. Kaplan, C. R. Safuya, A. Lindegaard-Andersen, S. Mathesen, Phys. Rev. B 22, 312 (1980)
[2] J. Salinger, R. Bruinsmen, Phys. Rev. A 43, 2910 (1991)
[3] I. G. Voigt-Martin, H. Krug, D. Van Dyck, J. Phys. (Fr) 51,2347 (1990)
[4] H. Hauptmann, Crystal Structure Determination, Plenum Publish., New York
[5] G. Bricogne, Acta Cryst. (1986)
[6] D. Dorset, Ultramicroscopy 38, 23 (1991)
[7] W. Dong, T. Baird, J. R. Fryer, C. Gilmore, D. D. MacNicol, C. Bricogne, D. J. Smith, M. A. O'Keefe, S. Hovmöller, Nature 355
[8a] I. G. Voigt-Martin, D. H. Yan, C. Gilmore, Manuscript in preparation for Ultramicroscopy
[8b] R. Henderson, J. M. Baldwin, T. Ceska, F. Zemlin, E. Beckman, K. Downing, J. Mol. Biol. 213, 899, (1990)
[8c] S. Hovmöller, Ultramicroscopy 41, 121, (1992)
[9] I. G. Voigt-Martin, H. Durst, B. Reck, H. Ringsdorf, Macromolecules 21, 1620 (1988)
[10] I. G. Voigt-Martin, H. Durst, Macromolecules 22, 168 (1989)
[11] I. G. Voigt-Martin, M. Schumacher, R. W. Garbella, Macromolecules 25, 961 (1992)
[12] I. G. Voigt-Martin, H. Durst, Liquid Crystals 2, 585 (1987)
[13] I. G. Voigt-Martin, D. H. Yan, Proceedings of the Electron Microscopical Society of America 1993
[14] J. Cowley, Diffraction Physics, North Holland Elsevier Science Publishers 1984

[15] D. Van Dyck, W. Coene, Ultramicroscopy 15, 29 (1984)
[16] D. Adam, F. Closs, T. Frey, D. Funhoff, D. Haarer, H. Ringsdorf, P. Schumacher, K. Siemensmeyer, Phys. Rev. Lett. 70, 457 (1993)
[17] S. Chandrasekhar, Liquid Crystals, Cambridge University Press (1977)
[18] G. S. Ranganath, Rep. Prog. Phys. 53, 57 (1990)
[19] C. Destrade, P. Foucher, H. Gasparoux, N. H. Tinh, A. M. Levelut, J. Malthete, Mol. Cryst. Liq. Cryst. 106, 121 (1984)
[20] A. M. Levelut, J. Chem. Phys. 88, 149 (1983)
[21] A. J. Leadbetter, Critic. Rep. on Applied Chem. 22, Ed. G. W. Gray, Chichester, Wiley
[22] H. Ringsdorf, P. Tschirner, O. Herrmann-Schönherr, J. H. Wendorff, Makromol. Chem. 188, 1431 (1987)
[23] P. A. Heiney, E. Fontes, W. de Jeu, A. Riera, P. Carroll, A. B. Smith, J. Phys. (Fr) 50, 461 (1989)
[24] R. Wüstefeld, Ph. D. Thesis, Universität Mainz, FRG (1990)
[25] W. Kranig, Ph. D. Thesis, Universität Mainz, FRG (1990)
[26] J. J. P. Stewart, J. Comput. Chemistry 10, 221 (1989)
[27] I. G. Voigt-Martin, M. Schumacher, R. W. Garbella, American Crystallographic Association Symposium Pittsburgh 1992
[28] R. Henderson, J. M. Baldwin, K. Downing, J. Lapault, F. Zemlin, Ultramicroscopy 19, 147 (1968)
[29] R. B. Meyer, L. Liébert, L. Strzelecki, P. Keller, J. Phys. (Fr) Lett. 36: L69, (1975)
[30] Ferroelectric Liquid Crystals, Ed. G. W. Goodby et al., Gordon and Breach Science Publishers 1992
[31] L. A.Beresnev, L. M. Blinov, M. A. Osipov, S. A. Pikin, Mol. Cryst. Liq. Cryst. 158A, 1 (1988)
[32] G. Scherowsky, A. Schliwa, J. Springer, K. Kühnpast, W. Trapp, Liq. Cryst. 5, 1281 (1989)
[33] H. Poths, A. Schönfeld, R. Zentel, F. Kremer, K. Siemensmeyer, Adv. Mater. 4, 351 (1992)
[34] F. Kremer, S. U. Vallerien, R. Zentel, Adv. Mater. 2, 145 (1990)
[35] M. Honig, R. W. Garbella, I. G. Voigt-Martin, H. Poths, R. Zentel, 22. Freiburger Arbeitstagung Flüssigkristalle (1993)
[36] M. Ballauf, Angewandte Chemie 101, 261 (1989)
[37] I. G. Voigt-Martin, P. Simon, R. W. Garbella, H. Ringsdorf, P. Tschirner, Macromol. Chem., Rapid Commun. 12, 285 (1991)
[38] M. Ebert, O. Herrmann-Schönherr, J. H. Wendorff, H. Ringsdorf, P. Tschirner, Liq. Cryst. 7, 63 (1990)
[39] M. Ballauf, J. Polym. Sci. (Phys) 25, 739 (1987)